Chapter 2

Objects of Investigation

C_{60} fullerenes and model peptides in the gas phase are the objects of interest in this work. Due to its well defined highly symmetric structure, 174 nuclear degree of freedom, 240 valence electrons (60 essentially equivalent delocalised π electrons and 180 structure defining localised σ electrons), C_{60} may be considered as a model of large finite molecular systems for studying of complex photo physical processes. Model peptides are an excellent example of a system for studying selective bond breaking and rearrangement. Such investigations open the door to new applications in biology and medicine. Gas phase studies of such objects provide a direct access to isolated molecules free from interactions with the environment. Indeed, the dielectric constant of protein powders is around 24 only [SBr96]. This contrasts with liquid water which has a dielectric constant of ≈ 80 at room temperature and pressure. Therefore, physical properties of large biological molecules studied in water solutions may be influenced strongly by the interaction with the highly polarisable water molecules, while experiments in vacuum may sometimes mimic the true behaviour of biological molecules in a protein environment much better.

This chapter gives a general description of physical properties of these two many-body systems and methods of their investigations in the gas phase.

2.1 C_{60} Fullerene and its Properties

Two main allotropic forms of bulk carbon are graphite and diamond. Carbon clusters, which possess many unique properties, constitute another allotropic form. Small carbon clusters (C_n, $n \leq 9$) exist in linear chains as the most stable form [RCK84]. Larger clusters (C_n, $9 < n < 30$)

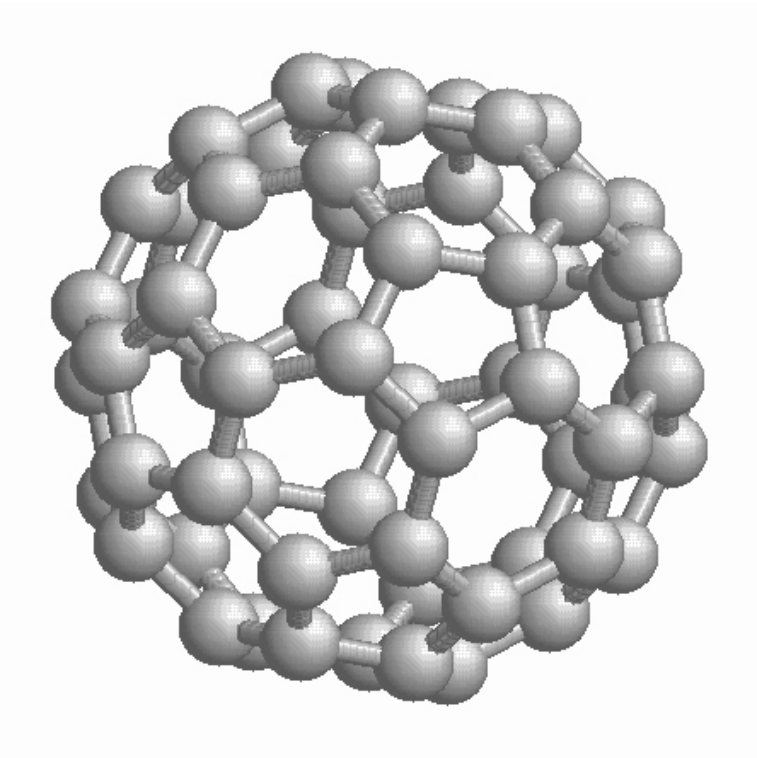

Figure 2.1: The structure of C_{60} fullerene.

are also found in ring structure of carbon atoms [HHK91]. Larger clusters (C_n, $n > 30$) have a cage structure of fullerenes formed by rings of hexagons and pentagons [LCX99]. According to the Euler's theorem for polyhedra [FMR93] any fullerene must have 12 pentagonal faces and an arbitrary number of hexagonal faces. Since the addition of an extra hexagon appends two carbon atoms, all fullerenes have an even number of carbon atoms.

The C_{60} fullerene was discovered by Kroto, Smalley, Curl, and collaborators in 1985 [KHO85] and was rewarded by the Nobel prize in 1996. Due to the closed cage structure and high symmetry C_{60} fullerene is much more stable in comparison to its neighbours [FMa92]. The structure of C_{60} fullerene is shown in Fig. 2.1. The cage is built out of 12 pentagonal and 20 hexagonal faces representing a truncated icosahedron. A regular truncated icosahedron has 90 edges of equal length and 60 equivalent vertices. Each carbon atom is trigonally bonded to three other carbon atoms by sp^2 bonds. The curvature of the C_{60} cage leads to some admixture of sp^3 bonding. The three bonds are not equivalent. Two bonds on the pentagonal edges are electron-poor single bonds. While the bonds joining two hexagons are electron-rich double bonds. The lengths of single and double bonds are $1.46\,$Å and $1.40\,$Å, respectively

[JMB90]. Since the lengths of single and double bonds are not exactly equal the C_{60} cage is not a regular truncated icosahedron. Nevertheless, due to the small difference between the single and double bounds, the cage can be considered as a regular structure. The diameter of C_{60} fullerene based on the geometrical consideration and assuming the carbon atom as points is 7.09 Å. The diameter of C_{60} experimentally measured with NMR technique is 7.10 ± 0.07 Å [JBY92]. Taking into account the size of the π electron cloud associated with the carbon atoms on the C_{60} cage, an estimate of the C_{60} outer diameter is 10.34 Å [DDE96].

A truncated icosahedron belongs to the I_h point symmetry group. It has 10 irreducible representations and 120 symmetry operations which can be grouped into 10 classes [DDE96]. Many special properties of C_{60} fullerene are directly related to its highly symmetric structure.

C_{60} has 174 vibrational degrees of freedom which due to the icosahedral symmetry relate to 46 distinct mode frequencies only. These modes have the symmetries

$$\begin{aligned} &2A_g[1] + 3F_{1g}[3] + 4F_{2g}[3] + 6G_g[4] + 8H_g[5] + \\ &+A_u[1] + 4F_{1u}[3] + 5F_{2u}[3] + 6G_u[4] + 7H_u[5] \quad , \end{aligned} \tag{2.1}$$

where the multiplicities indicate a number of distinct mode frequencies, the symmetry labels relate to irreducible representations of the icosahedral symmetry group, the subscripts g and u refer to the symmetry of the eigenvector upon the action of the inversion operator, and the numbers in brackets indicate the degeneracy of each mode symmetry.

Carbon has two stable isotopes: ^{12}C with a natural abundance of 98.89% and ^{13}C with an abundance of 1.11%. Thus, there is a high probability of finding one or more ^{13}C atoms in a C_{60} molecule. The probability $p(r)$ for r isotopic substitutions in a C_{60} fullerene is given by

$$p(r) = \binom{60}{r} x^r (1-x)^{60-r} \quad , \tag{2.2}$$

where x is the ^{13}C isotope abundance. Assuming $x = 0.01108$ [DDE96] the probabilities to find 0, 1, 2, 3, or 4 ^{13}C atoms in the C_{60} molecule are 0.5125, 0.3445, 0.1139, 0.0247, and 0.0039, respectively. The presence of ^{13}C isotope lowers the symmetry of the fullerene and introduces various isotope effects such as, for example, the modification of the rotational levels of C_{60} [HRe92].

Methods for studying the vibrations of C_{60} fullerene include Raman and infrared spectroscopy, inelastic neutron scattering, luminescence, and electron energy loss spectroscopy [JMD92]. Among these methods Raman and infrared spectroscopy allow one to obtain the

Table 2.1: Optically active vibrational modes of C_{60} fullerene obtained with the first order Raman and infrared spectroscopy (the values are taken from [DZH93, WRE93]).

Mode	Frequency, cm^{-1}	Period, fs	Type of the activity
$A_g(1)$	497.5	67.0	Raman
$A_g(2)$	1470.0	22.7	Raman
$H_g(1)$	273.0	122.1	Raman
$H_g(2)$	432.5	77.1	Raman
$H_g(3)$	711.0	46.9	Raman
$H_g(4)$	775.0	43.0	Raman
$H_g(5)$	1101.0	30.3	Raman
$H_g(6)$	1251.0	26.6	Raman
$H_g(7)$	1426.5	23.4	Raman
$H_g(8)$	1577.5	21.1	Raman
$F_{1u}(1)$	526.5	63.3	infrared
$F_{1u}(2)$	575.8	57.9	infrared
$F_{1u}(3)$	1182.9	28.2	infrared
$F_{1u}(4)$	1429.2	23.3	infrared

most precise values for the vibrational frequencies. Only A_g and H_g symmetry modes are Raman active. The infrared active modes have F_{1u} symmetry. Therefore, C_{60} in the ground state exhibits 10 Raman active ($2A_g$ and $8H_g$) and 4 infrared active ($4F_{1u}$) modes. Vibrational frequencies and periods of the optically active modes derived from first order Raman and infrared spectra are summarised in Table 2.1. The remaining 32 modes are not active in first order Raman and infrared spectra. Nevertheless, many of these silent modes can be observed in higher order Raman [DZH93] and infrared [WRE93] spectra, by inelastic neutron scattering [CJB92], or by electron energy loss spectroscopy [GYP92].

Several vibrational modes are especially important in the excitation with an intense fem-

tosecond laser radiation namely the $A_g(1)$, $A_g(2)$, and $H_g(1)$ modes. However, excitation at high intensities implies mechanisms quite different from conventional, optical dipole induced infrared absorption or Raman processes: in fact, the excitation of these modes (at least at intensities range used in the present work) is due to non-adiabatic multielectron dynamics (NMED). The $A_g(1)$ "breathing" mode ($497.5\,\mathrm{cm}^{-1}$) involves symmetric radial displacement of all 60 carbon atoms with an equal amplitude. The $A_g(2)$ "pentagonal pinch" mode ($1470.0\,\mathrm{cm}^{-1}$) corresponds to primarily tangential displacements with a contraction of the pentagonal rings and an expansion of the hexagonal rings. The $H_g(1)$ "prolate-oblate" mode ($273.0\,\mathrm{cm}^{-1}$) involves an elongation of the cage along one axis. Theoretical simulations [TNE01] indicate that the interaction of C_{60} with moderately intense laser radiation centred at $620\,\mathrm{nm}$ and a pulse duration of $10\,\mathrm{fs}$ leads to the excitation of both $A_g(1)$ and $A_g(2)$ modes. The $A_g(2)$ mode dominates at the laser intensity of $0.56 \times 10^{12}\,\mathrm{W/cm^2}$, while at higher intensities the $A_g(1)$ mode prevails over the $A_g(2)$ mode. At the intensity of $1.5 \times 10^{12}\,\mathrm{W/cm^2}$ the $A_g(1)$ mode is found to be completely dominant. Recently, numerical results showed that the duration of the exciting laser pulse may determine which mode is most prominently excited [ZGe04]. It was found that for laser photon energies from 0.5 to $1.6\,\mathrm{eV}$ and pulse durations shorter than $40\,\mathrm{fs}$ the A_g modes dominate, while for longer pulses the $H_g(2)$ mode take over. The $H_g(1)$ mode dominates over the laser excitation of C_{60} with intense ($\sim 3 \times 10^{14}\,\mathrm{W/cm^2}$) pulses centred at $1500\,\mathrm{nm}$ with a duration of $70\,\mathrm{fs}$ [BCR03]. In this case the excitation mechanism is also specific to strong field interaction but different to the one at shorter wavelengths [NKS07].

According to the theoretical prediction [SNS06, SNS06a] ionisation as well as excitation of C_{60} weakens the bonds between the carbon atoms and has an influence on frequencies of the vibrational modes. For example, at a laser intensity of $5 \times 10^{13}\,\mathrm{W/cm^2}$ nearly 31 valence electrons are strongly excited resulting in an impulsive force that expands the C_{60} fullerene dramatically up to $9.4\,\text{Å}$ which is 130% of its ground state diameter [LSS07]. This leads to a rise of the vibrational period which depends on the excited electronic configuration and therefore on the absorbed energy.

In a molecular orbital (MO) picture the $180\,\sigma$ binding electrons of C_{60} have energies $3-6\,\mathrm{eV}$ below the Fermi level, while $60\,\pi$ electrons with higher lying energy levels near the Fermi level define the electronic structure. Many efforts were made to describe the electronic structure of the fullerene molecule. Various theoretical methods have been suggested [DDE96] starting

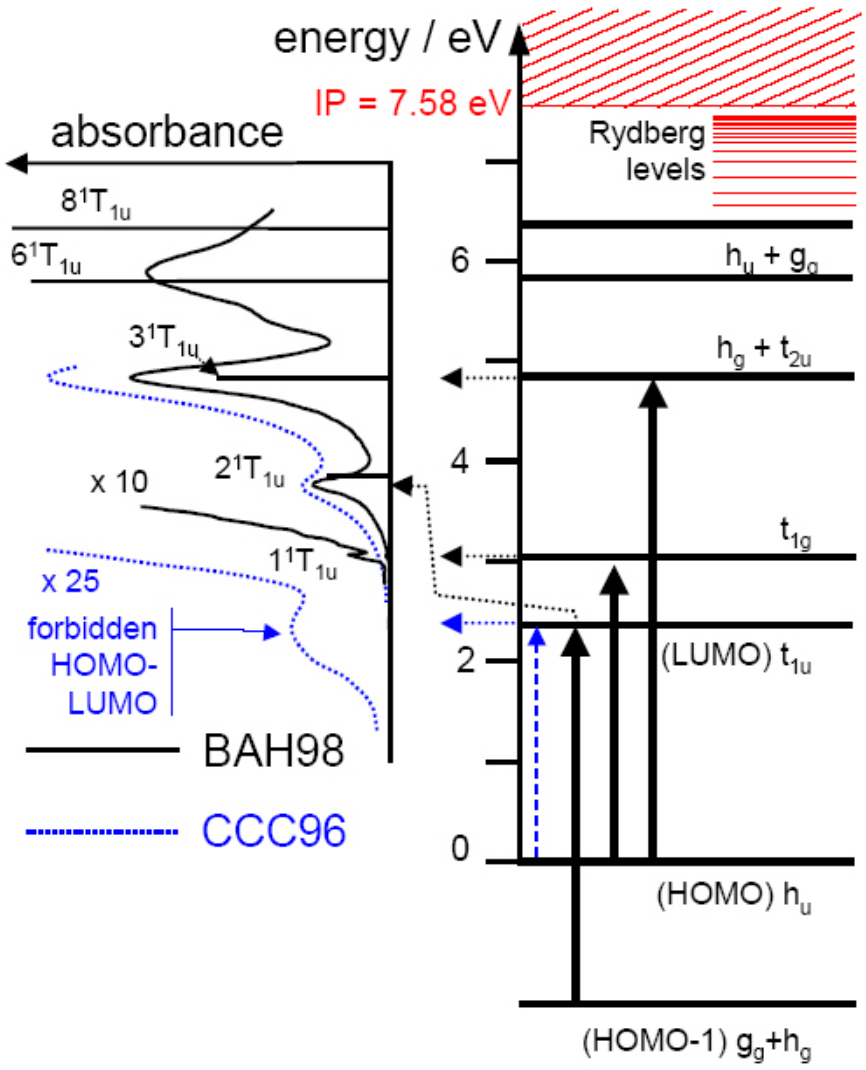

Figure 2.2: Single electron energy diagram and electronic absorption spectra of C_{60} fullerene (the data and picture are taken from [CCC96, BAH98], and [HLS05], respectively).

from one electron Hückel calculations to first principle models [Had92]. The high symmetry of the C_{60} molecule may even allow one to use simple phenomenological approaches for finding the electronic structure based on symmetry considerations with satisfactory results. One may, e.g. start with a spherical shape of the C_{60} molecule and introduce the icosahedral symmetry of the C_{60} fullerene as a perturbation [SDD92].

In the most simple model, often used with success in dynamical calculations, one treats the π electrons in a spherically symmetric shell potential (jellium model) [PNi93]. Then, according to the Pauli principle the states with an angular momentum up to $l = 4$ are populated by 50 π electrons, while the remaining 10 of π electrons occupy the states with $l = 5$ which can admit

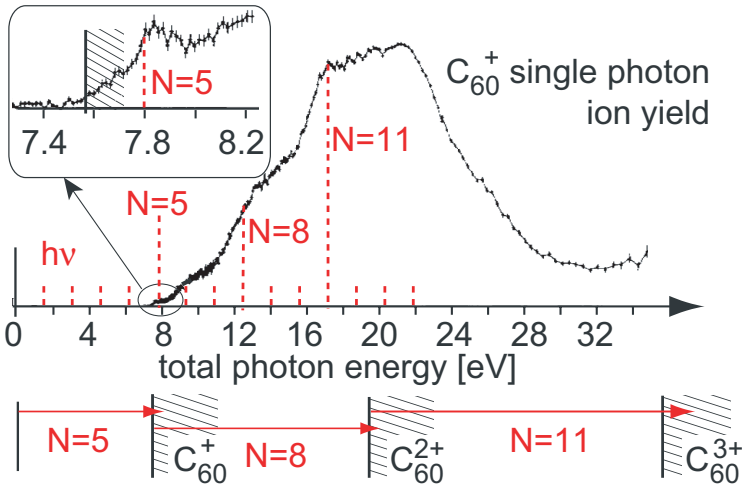

Figure 2.3: Illustration of the energetics for plasmon enhanced multiphoton process in the generation of C_{60}^{q+} with different final charge state q (adopted from [HSV92]). Dashed vertical lines indicate photons energies $N\hbar\nu$ ($\hbar\nu$=1.56 eV) required for the sequential ionisation.

up to 22 electrons in total. These 10 filled substates correspond to the completely filled h_u level leaving the t_{1u} and t_{1g} levels unoccupied. Thus, the highest occupied molecular orbital (HOMO) is the h_u level, while the lowest unoccupied molecular orbital (LUMO) corresponds to the t_{1u} level. The value of the HOMO-LUMO gap according to the density-functional theory in the local-density approximation (DFT-LDA) is 1.79 eV [CCY97].

The energetic positions of these levels in the MO picture are indicated in the right part of Fig. 2.2. In the left part of Fig. 2.2 these MO levels are correlated with the corresponding *ab initio* calculated energies of the electronic states of C_{60}. This is compared with the optical absorption spectrum which, in principle, gives the most direct information on the electronic properties of C_{60}. Since the HOMO and LUMO states posses the same odd parity an electron dipole transition between these single electron states is forbidden by parity considerations. The first electric dipole allowed optical transition is between the HOMO and "LUMO+1" states. The solid black line in the left part of Fig. 2.2 reproduces a measurement in the hexane solution [BAH98], while the blue dotted line corresponds to gas phase studies [CCC96]. Unfortunately, both spectra show essentially identical broad bands owing to the many internal degree of freedom.

Due to the large number of valence electrons in a single C_{60} molecule multielectron effects can play an important role. The evidence of multielectron effects was proven in one photon

ultraviolet excitation of the giant plasmon resonance centred at $20\,\mathrm{eV}$ using synchrotron radiation [HSV92]. This plasmon resonance is shown in Fig. 2.3 and is attributed to the collective motion of the valence electrons of C_{60}^{+}. The excitation of multiple electrons may also be possible with strong fs laser fields [LBR01].

Ionisation and fragmentation of C_{60} fullerenes investigated intensively by means of photoelectron spectroscopy and mass spectrometry. There is a large variety of experimental methods based on the excitation of C_{60} by single photon [YRB92] or multiphoton [OHC88] absorption, electron impact [FFM98], collisions with neutral particles [Tak92], atomic [WCV94] and molecular [VHC98] ions. Moreover, time resolved techniques provide a powerful tool for studying the dynamics of relaxation processes within the C_{60} molecule [BHS04]. Photoinduced ionisation and fragmentation of C_{60} fullerenes are discussed in Chapter 8 and Chapter 9 at great length.

2.2 Model Peptides and Methods of Investigations

In recent years, great interest in studying of biological molecules has been demonstrated [WHC03, JES04, JJC06, VHo07]. Among the different methods for analysis of structure, function, and electronic properties of these molecules spectroscopical methods in the gas phase can be considered as the most powerful and promising techniques. Gas phase investigations are not only ideally suited for studying isolated molecules and comparison with theoretical predictions but also allow one to distinguish intrinsic properties of single molecules from their properties in condensed phases. The low thermal stability of many biomolecules creates significant problems in their investigation in the gas phase. There are several practical techniques to transfer biological molecules into the gas phase such as thermal evaporation in an oven [SRK00], thermospray [RPL85], electrospray [YFe84] laser induced ablation [LLu88], or matrix assisted laser desorption (MALDI) [Lev94]. The molecules thus prepared usually possess rather high vibrational and rotational energy. That can be a problem for a careful analysis of their properties. Therefore, an isolation of biomolecules into large helium clusters [LTV99] or, more generally, a combination with a seeded supersonic expansion of a rare gas [MAL92] is applied to cool down the molecules. Collisions with rare gas atoms, which are cold due to the adiabatic expansion, effectively cool the vibrational and rotational degrees of freedom of the biomolecules, if carefully done without condensation.

Gas phase studies of biological molecules can be performed with mass, isomer, and state selective spectroscopic methods. Moreover, modern femtosecond lasers provide a tool for time resolved investigations of the various intermediates during photochemical reactions, protein folding, or other biochemical processes [ANO06, YKE07, YST07]. One may distinguish two groups of methods: those based on optical spectroscopy and those based on the mass spectrometry.

Classical method of optical spectroscopy mostly rely on laser induced fluorescence (LIF), where the fluorescence yield is detected after excitation of (biological) molecules in the near ultraviolet range [Kam05]. An assignment based on power saturation studies of vibrationally resolved LIF spectra provides information about stable conformations of these molecules present in the gas pase at low temperature [Zwi01]. The main limitation of this method is imposed by the weak quantum yield for many biological species. A second method of optical spectroscopy applied to biomolecules is so-called "infrared cavity ring-down laser spectroscopy" (IR-CRLAS) [CPP98]. The IR-CRLAS is an absorption spectroscopic technique combining high sensitivity and high spectral resolution. It is based on measurements of the exponential decay of the intensity of laser radiation trapped in a high reflective optical cavity with an absorbing sample inside. The absolute absorbance of the sample is directly derived from the measured time constant of the exponential decay.

To generate ions of biomolecules in mass spectroscopy one may e.g. use laser ionisation or fast atom bombardment [BMa87, Bie92]. This allows one not only to determine molecular weight of biological molecules but it may also help to distinguish between different structural peculiarities of the molecules. More structural information can be obtained by utilising of a tandem mass spectrometer, involving two ore more mass spectrometers [RYM95]. The first spectrometer is used to select the ions of interest, while the second device detects all fragments produced after additional excitation of the selected precursor ions. This method allows one to analyse molecules mixtures without the necessity to separate individual components before the analysis [Pap95].

Recently new combinations of spectroscopical techniques were successfully applied to map conformational landscapes of small biomolecules and biomolecular clusters [SSP05, CPD06, POo07]. If the object of investigation contains an aromatic chromophore, the combination of infrared excitation with resonant two photon ionisation (IR/R2PI) is ideally suited to in-

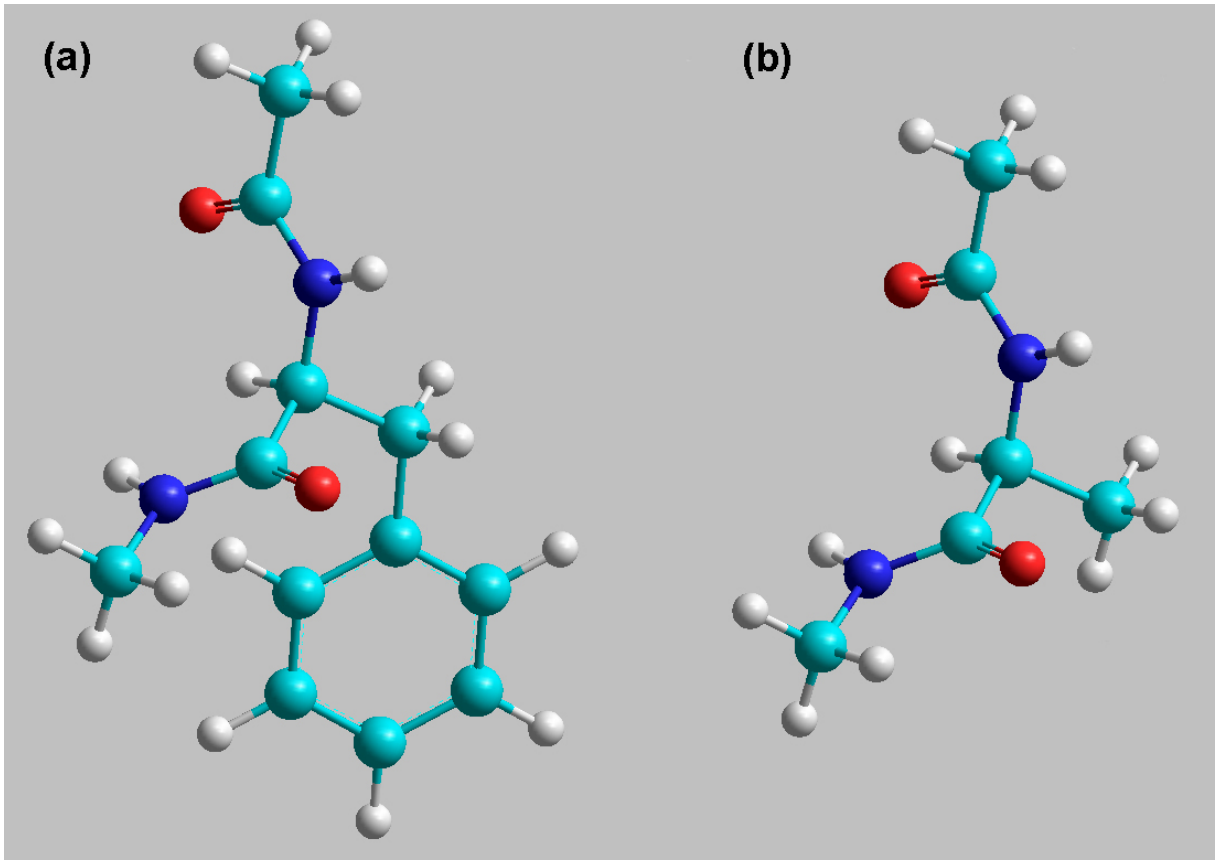

Figure 2.4: Model peptides used in present work: (a) Ac–Phe–NHMe; (b) Ac–Ala–NHMe.

vestigate the infrared spectra of different neutral biomolecules in the ground electronic state [WVN04]. This method is mass and isomer selective due to the R2PI process. Moreover, the combination of the IR/R2PI method with *ab initio*, density functional theory (DFT), or Hartree-Fock (HF) calculations allows one to identify different conformational structures [BFG06]. The second powerful method is based on the combination of ultraviolet hole burning and R2PI [SMZ07]. This combination reveals the overlapping spectral features which correspond to different conformers or clusters.

In the present work ionisation and fragmentation of two molecular systems Ac–Phe–NHMe and Ac–Ala–NHMe after the excitation with intense, shaped laser pulses are studied with time of flight mass spectrometry. The amino acid complex Ac–Phe–NHMe is obtained from the amino acid phenylalanine by introducing an acetyl group to protect[1] the base NH_2 and by using the amide group instead of the pure acid as shown in Fig. 2.4a. Thus, Ac–Phe–NHMe contains

[1] A protecting group is any chemical moiety that replaces a highly reactive functional group in a molecule to protect this functional group from unwanted chemical interactions.

a –CO–NH–CHR–CO–NH– moiety, the structural key element of all peptides. The second amino acid complex Ac–Ala–NHMe has alanine instead the chromophore phenylalanine, while the backbone structure with the protection groups is uncharged (Fig. 2.4b). Both molecules systems contain CH–CO, CO–NH, and N–C_α bonds as well as side chains and therefore may be regarded as models of small peptides.